International Journal of Engineering Research and Technology. ISSN 0974-3154, Volume 14, Number 8 (2021), pp. 773-781

Classification of Healthy Persons and Persons with Ulnar Syndrome by Means of Electromyographic Signals Feeding an Artificial Neural Network

Diego Alejandro Barragán Vargas[1], Roberto Ferro Escobar [2] and Jorge Enrique Salamanca Céspedes[3]*

[1]Universidad Distrital Francisco José de Caldas; ORCID: 0000-0003-3069-4712

[2] Universidad Distrital Francisco José de Caldas; rferro@correo.udistrital.edu.co; ORCID: 0000-0002-8978-538X

[3] Universidad Distrital Francisco José de Caldas; jsalamanca@udistrital.edu.co; ORCID: 0000-0002-9396-2641

Abstract

The paper briefly explains the basic concepts of electromyography, the electrical model of a peripheral nerve, the basic characteristics of the hand and the ulnar syndrome, and then explains the visualized parameters that form the database that allowed the design of the artificial neural network. Subsequently, the design of the neural network is detailed and compared with different optimization methods and with different linear functions. Finally, it is shown that the best architecture obtained was [2 2 1] by means of the Levenberg Marquardt optimization algorithm, which presented an MSE of 4.6E-05, an MAE of 32% and a correlation of 0.9998. As a future work, it is desired to generate a complete electronic prevention system focused on carpal tunnel syndrome, which allows generating its own data for the generation of a more robust neural network that allows observing different variables and the weight of each of the inputs, in order to obtain a reliable output of the computational model to be tested. It is important to note that the article is one to the results of the development currently carried out to the master's degree in engineering with an emphasis on electronics carried out in the University Distrital Francisco José de Caldas.

Keywords: Artificial Neural Network; Electromyography; Hand; Cubital Tunnel Syndrome.

1. INTRODUCCIÓN

A search was made for documents that would explain in a simple way the concepts discussed in the article, such as electromyography, which is an electrophysiological study of the neuromuscular system [1][2][3][4][5], it is also a biomedical measuring instrument in which an examination of the electrical activity of a motor unit is performed with the aim of determining the site of injury of a peripheral nerve or spinal nerve roots [6][7], it is also frequently used to study muscle diseases [8][9][10]; There are two types of electromyography, a superficial one that is by means of surface electrodes and an invasive electromyography where the study is generated by means of needles [11]. Figure 1 details a way of measuring surface electromyography.

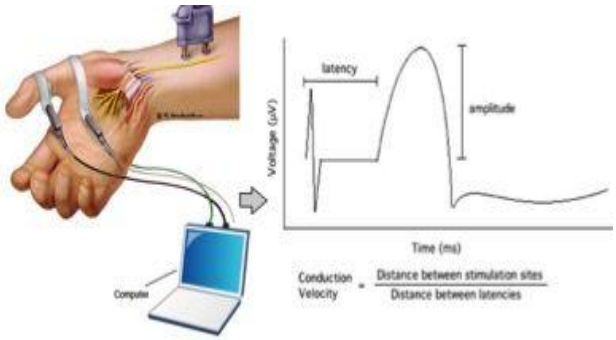

Figure 1. Electromyography [12]

Different authors have tried to design electrical models of the nerve, by means of resistors, capacitances, inductances and current or voltage dependent sources [13], in addition they have studied and made several models of nerves with myelin and without myelin to understand the behavior of a healthy nerve and a nerve that has lesion [14] [15], an example of this is given in [16], where a general model made by Hodgkin and Huxley is observed where it is visualized that the behavior of a membrane can be represented by the electrical circuit of illustration 2, where the current can be transported through the membrane by charging the capacitance of the membrane or through the movement of ions by means of the nonlinear conductance in parallel with the capacitance of the membrane, the equation that describes this model is:

$$I = I_{C_m} + I_K + I_{Na} + I_L \quad (1)$$

That upon further detailing you have:

$$I = C_m \frac{dV_m}{dt} + g_k n^4 (V_m - V_k) + g_{Na} m^3 h (V_m - V_{Na}) + g_L (V_m - V_L) \quad (2)$$

Where the equation I is the total ionic current across the membrane due to ion flux, Cm is the membrane capacitance per unit area gk and gNa are the conductances of sodium and potassium channels respectively, gL is the conductance of chloride or other elements and Vm is the potential across the membrane.

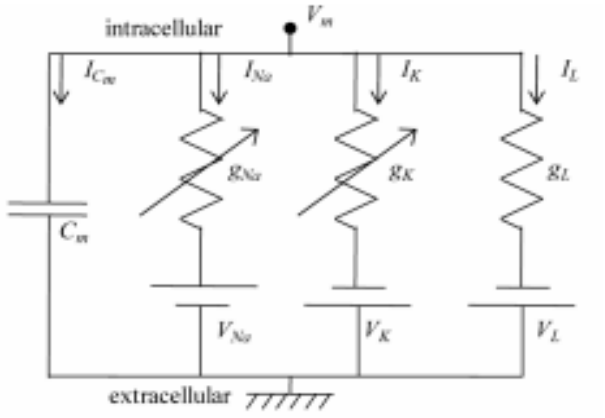

Figure 2. Equivalent electrical circuit of a membrane **[16]**

Bearing in mind the previously mentioned concepts, we can now visualize the hand, which is an organ that is part of the extremities of the human body for physical interaction and manipulation with the environment, located at the ends of the forearms [17], it is also one of the parts of the body with greater use in daily life, so it is exposed to injury by disease or accidents during daily activities that are performed at work or at home [18], The analysis of this is essential for various applications that can range from sports performance, to an analysis of computer-human interaction, this is due to the great variety and adaptability of their movements that are due to the complex mechanical structure that has, which includes bones, ligaments, muscles, tendons, soft tissues and skin [19]. It is important to note that the skeletal model of the hand has 23 degrees of freedom internally [20]. A disease that significantly affects the hand is cubital tunnel syndrome which is the second most frequent neuropathy after carpal tunnel syndrome, so it is a reason for consultation for elbow surgery and sometimes hand surgery [21], this is because the ulnar nerve can be compressed in several parts, however, in [22] it is commented that in the flexor capri ulnaris is where this compression is most frequently observed.

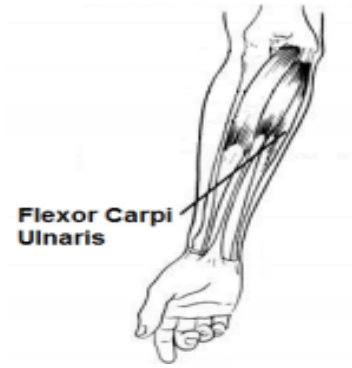

Figure 3. Flexor Capri Ulnaris **[23].**

The information acquired from the electromyographic signals of the ulnar nerve that innervates the hand, will be essential to run the artificial intelligence (AI) algorithm that will be exposed in the course of the document, it is important to note that there are several definitions that try to explain the AI, an example is Jhon McCarthy which says that AI is the science and engineering to make intelligent machines, another important example is Eugene Charniak who expresses that AI is the study of mental faculties through the use of computational models and also Marvin Minsky who comments that artificial intelligence is the construction of computer programs that perform tasks, for the moment efficiently executed by humans because they require high-level mental processes such as: perceptual learning, memory organization and critical reasoning [24]. One field of artificial intelligence is artificial neural networks, which by means of their neurons perform information processing, for this purpose the neurons are connected to each other by means of weighted connections [25], as visualized in the following figure:

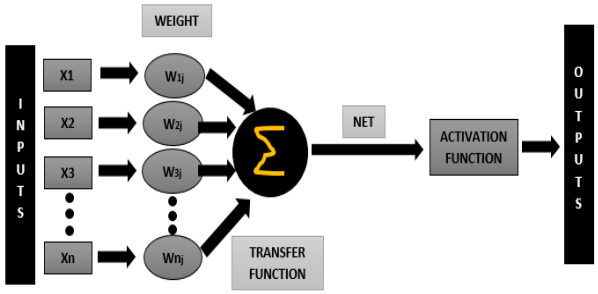

Figure 4. Structure of an artificial neural network **[25].**

In 1943 McCulloch and Pitts made the model of an artificial neuron, generating the description of the physiological system followed by a biological neuron at the synapse, this abstract and simple model of a neuron is as shown in Figure 6, which is the basic processing element in an artificial neural network [26] [27]. Neural networks have the inherent capability in nonlinearity approximation and pattern recognition without the requirement of prior knowledge of the system parameters [28].

The model is composed of a vector of weights W=(W1j, W2j, W3j...,Wnj), where W1j is the threshold of action or activation, in figure 4 we can observe the output of the neuron that for this case will be called Y, the activation function U, the inputs X=(X1,X2,X3,...,Xn), the mathematical model for a single neuron is shown below:

$$Y = U(\sum_{i=1}^{m} X_i W_i - W_0) \quad (3)$$

2. Sample Space and Data Processing

To understand what is the sample space of this experiment, it is first necessary to express that the database was acquired from the machine learning repository of the UCI which was supported by [29] for the acquisition of the same, these data were collected at a sampling frequency of 500Hz, in addition to acquiring the signal by means of two differential EMG sensors that in the end were displayed in two channels, the protocol that was followed in [30] consisted of several experiments of free and repeated grasping with different elements, which were essential for the realization of the different movements of the hands. The two EMG surface

electrodes placed them on the forearm, one on the flexor Capri Ulnaris and the other on the extensor Capri Radialis, held by elastic bands and a third reference electrode placed it in the middle for the collection on muscle activity. It was also reviewed [31-33] to understand more about the hand grip performance. The information present in the database is in voltage values and is classified into six different movements performed by the hand, depending on the grip which can be a spherical, tip, palm, lateral, cylindrical or hook grip, in this paper we analyzed the database containing the voltage values of channel 1, which showed 5 different subjects (two males and three females) which repeated 30 times each grip for 6 seconds.

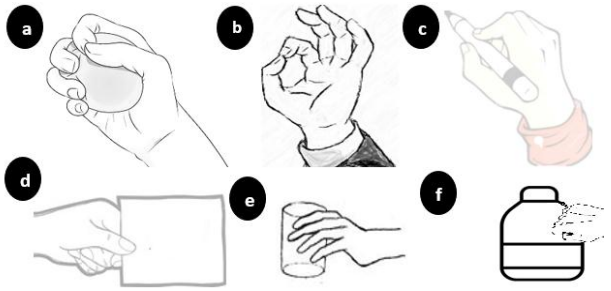

Figure 5. Hand exercise design design bocketting

Visualizing illustration 5 it can be observed that the sample space is conformed in the following way:

$$\Omega = \{H_a, H_b, H_c, H_d, H_e, H_f\} \quad (4)$$

The sample space described in equation 4 refers to the different possibilities of grasping the hand in the experiment (Figure 5). Now we proceed to generate two events, having:

$$A = \{H_a, H_c,\ H_e\} \quad (5)$$

$$B = \{H_b, H_d, H_f\} \quad (6)$$

Where A $\sqsubset$ Ω and B$\sqsubset$ Ω, which generates an event A with parameters obtained from the hand when grasping and exerting pressure on cylindrical and spherical objects and an event B with parameters obtained from grasping laminar elements, performing signs such as Ok visualized in Illustration 5b and grasping elements of considerable size. These are event fields F, which are classes of the subset of the sample space and satisfy the following axioms:

- F is non-empty.
- If A $\sqsubset$ Ω is such that $A \in F, A^c \in F$.
- If $A, B \sqsubset \Omega$ is such that $A, B \in F, A \cup B \in F$.

Finally, the power set of the experiment is:

$$|P(s)| = 2^{\Omega} = 2^6 = 64 \quad (7)$$

The cardinality of the sample space is 6. After the previous analysis, we proceeded to plot the EMG signals of the six cases described in Figure 5 of a patient from the database in MATLAB, obtaining the following graphs:

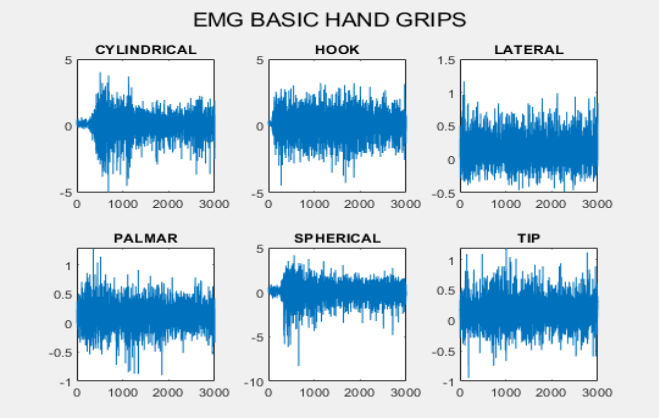

Figure 6. EMG signals of basic hand movements in mV.

In addition, it was reviewed in [34] that a person's normal values in EMG signals in their ulnar nerve are:

Table 1. Standard values of ulnar nerve motor fibers. [34]

Site of Estimulation	Amplitud (mV)	Latency (ms)	Difference Between Rigth and Left (ms)
Wrist	5.7±2.0	2.59±0.39	0.28±0.27
Below elbow	5.5±2.0	6.10±0.69	0.29±0.27
Above elbow	5.5±1.9	8.04±0.76	0.34±0.28
Axilla	5.6±2.1	9.90±0.91	0.45±0.39

Considering table 1, it was observed that the voltage tolerance is at 2mV for the wrist part which has a nominal value of 5.7mV, so the maximum value and minimum value were analyzed in the EMG database of the 30 repetitions performed by each participant obtaining the following tables:

Table 1. Maximum voltage values of the EMG signals of each participant.

SEX	CYL	HOOK	LAT	PALM	SPHER	TIP
F	4,56	4,68	1,32	1,55	5,66	2,47
F	4,13	6,85	3,69	7,18	7,19	3,36
F	1,83	9,96	1,02	1,35	8,05	0,86
M	1,39	6,32	1,78	0,58	2,19	0,74
M	2,16	1,75	3,51	4,43	2,67	5,64

In Table 2 it can be visualized that the maximum value for the cylindrical shape grip is 4.56mV and the minimum value is 1.39mV, the maximum value for the hook grip is 9.96mV and the minimum value is 1.75mV, the maximum value for a lateral grip is 3.69mV and the minimum value is 1.02mV, the maximum value for a spherical grip is 8, 05mV and the minimum value is 2.19mV and finally for the tip grip the maximum value is 3.36mV and the minimum value is 0.74mV, so we proceeded to generate more data above and below those values to simulate failed grips and possible hand failures, now we proceed to show the minimum values:

Table 3. Minimum voltage values of the EMG signals of each participant

SEX	CYL	HOOK	LAT	PALM	SPHER	TIP
F	-7,93	-7,07	-1,15	-1,74	-9,62	-1,64
F	-6,58	-9,69	-2,68	-4,69	-9,95	-2,73
F	-0,99	-9,87	-0,69	-0,95	-7,76	-0,49
M	-1,43	-4,62	-1,56	-0,31	-1,92	-0,44
M	-4,41	-2,25	-4,64	-7,48	-5,64	-9,64

Table 3 shows that the values are in the range [-0.99 -7.93] for cylindrical grip, [-2.25 -9.87] for hook grip, [-0.69 -4.64] for lateral grip, [-0.31 -7.48] for palm grip, [-1.92 -9.95] for spherical grip and [-0.44 -9.64] for tip grip, so we proceeded to generate random data above and below to simulate failed grips that could induce in hand response failures, which could be observed as failed action potentials expressing segmental demyelination or as muscle fatigue in which it requires more motor fibers to perform the same grip action [35]. Based on the commented values, we proceeded to the generation of a neural network with 12 inputs (6 maximum and 6 minimum values of each grip expressed in voltage), then we appended the output showing healthy users (database) and users with a possible hand condition (simulation taking into account the literature [34].

The data were then normalized using the following equation:

$$V_n = \frac{V - V_{min}}{V_{max} - V_{min}} \quad (4)$$

3. ALGORITHM DESIGN

The new database obtained after processing and treatment of the data was 680x13 resulting in 8840 data, the first step for the creation of the network was to use 70% of the data for training, i.e. 6188 data and 30% of the data for the corresponding validation, equivalent to 2652 data:

```
close all; clear all; clc
load('NORMALIZADOS.mat');
cont = 0;
%----------Training Data----------
x = NORMALIZADOS(1:476,1:12)'; %Input Matrix
y = NORMALIZADOS(1:476,1)';   %Output Matrix
%----------Validation Data----------
xx = NORMALIZADOS(477:680,1:12)';%Input Matrix
yy = NORMALIZADOS(477:680,1)';   %Output Matrix
nets = [];
```

Subsequently, we proceeded to create and train the network, to generate the construction of the universe of inputs, the objective function characteristic of each hidden layer of the neural network and thus also test the training algorithm, to continuously vary the number of neurons and hidden layers of the supervised neural network and thus obtain a suitable architecture to perform the classification, we also proceeded to calculate the mean absolute error, to determine the effectiveness of success of the classifying neural network, the part of the generated code that describes this part is as follows:

```
for h = 1:50
%%Creation and training of the network
PR = [0 1;0 1;0 1;0 1;0 1;0 1;0 1;0 1;0 1;0 1;0 1;0 1];
ARC = [2 2 1];
net = newff(PR, ARC,{'logsig' 'logsig' 'logsig'},'trainlm',
'learngdm','mse');
[net, tr] = train(net,x,y);
%% Validation (Error Calculation)
[Y] = sim(net,xx);
cont =0;
 for i=1:length(Y)
            if Y(i)<0.5
  Y(i)=0;
   else
            Y(i)=1;
   end
   if Y(i)==yy(i)
   cont = cont+1;
   end
   end
   errorpercent(h)= (203-cont)*100/203
   nets = [nets ; net];
end
```

4. RESULTS

The analysis of different neural network architectures was performed, generating a variation in the number of hidden layers, the number of neurons, the training algorithm, which for these tests were two, the first architectures were tested with the gradient descent algorithm (see Table 4) and the other architectures were designed with the Levenberg-Marquardt algorithm.

Table 2. Architecture with "TRAINGDA" training algorithm and "logsig" activation functions.

SIZE	NEURONS	MSE	MAE(%)	R
[2 1]	3	0,0019	33	0,9917
[3 1]	4	0,0017	33	0,9924
[5 1]	6	0,0018	32	0,9918
[7 1]	8	0,0011	33	0,9951
[2 2 1]	5	0,0029	32	0,9869
[2 3 1]	6	0,0042	32,7	0,9812
[5 3 1]	9	0,0017	33	0,9821
[7 5 1]	13	0,0011	33	0,9949
[12 7 1]	20	0,0011	33	0,9951
[2 2 2 1]	7	0,0025	32	0,9896
[7 5 3 1]	16	0,0016	32,7	0,9925

From Table 4 it was obtained that the best architecture for a neural network with one hidden layer is [5 1], for an architecture with two hidden layers is [2 2 1] and it was observed that as the number of layers and neurons increased the MAE was higher and generated a higher computational cost that delayed the training and validation so it was only simulated up to three hidden layers obtaining that the neural network of [2 2 2 2 1], was the network that obtained the lowest error.

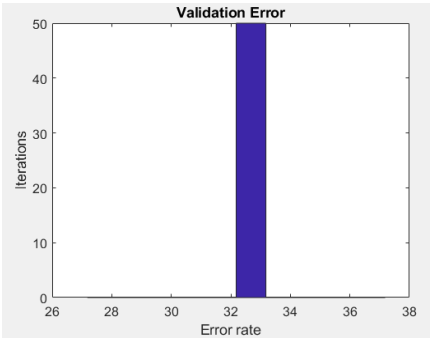

Figure 7. MAE error validation for the best hidden layer architecture of ARC [5 1]

Figure 7 shows that the MAE is 32%, which shows that it is not the best network for classifications, since this parameter indicates that out of every 10 people measured, approximately 3 will be misclassified, however, the computational cost is low and the training time of the artificial neural architecture is relatively short, since it took only two minutes to obtain the results of this network.

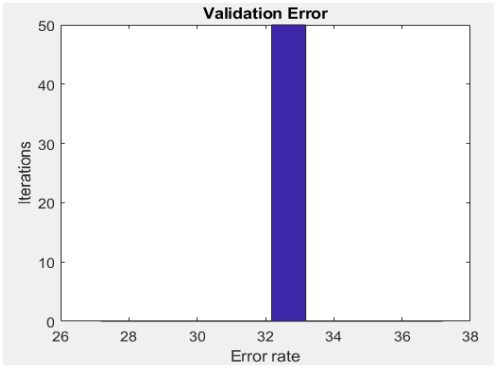

Figure 8. MAE error validation for the best two hidden layer architecture of ARC [2 2 1].

In Figure 8, it can be seen that the MAE is 32%, which shows that approximately out of every 10 evaluated for their respective classification, three will be wrong. The computational cost was similar to the case of the architecture [5 1], since the estimated training time was approximately two minutes.

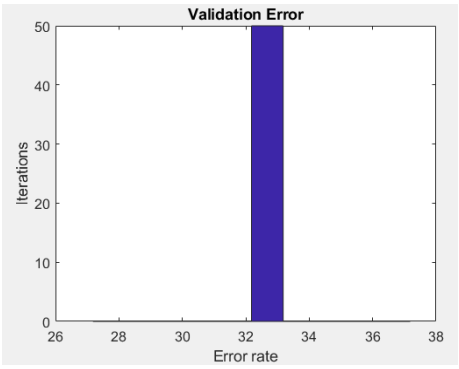

Figure 9. MAE error validation of major two-layer hidden architecture of ARC [2 2 2 1].

Figure 9 showed the best architecture obtained from neural networks with layers greater than 2, where it was observed that the MAE was 32%, similar to the architectures of one hidden layer and two hidden layers. The best architecture trained with the gradient descent algorithm was [5 1], then, other plots simulated in the MATLAB environment are shown, showing several characteristics of this neural network.

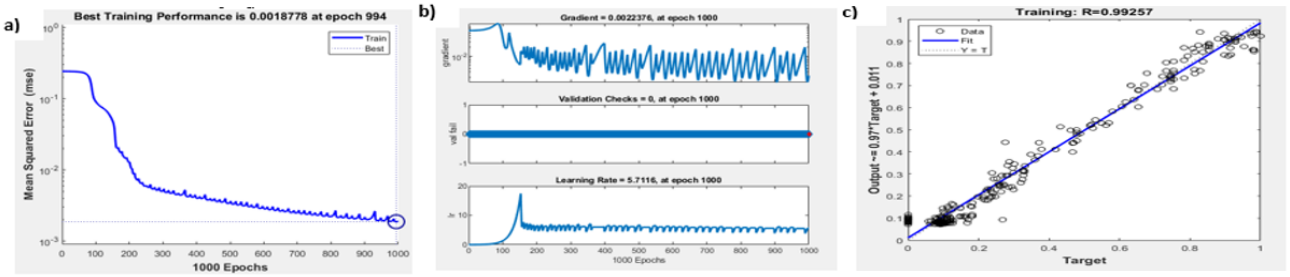

Figure 10. ARC [5 1], a) Mean square error MSE=0.0018, b) Gradient, validations and learning rate and c) Regression R=0.99257.

Table 5 shows the values obtained for the different architectures when simulating with the Levenberg-Marquardt training algorithm.

Table 3. Architecture with "TRAINLM" training algorithm and "logsig" activation functions.

SIZE	NEURONS	MSE	MAE(%)	R
[2 1]	3	5,6E-05	33	0,9997
[3 1]	4	3,1E-06	32,7	0,9999
[5 1]	6	2,5E-05	32,8	0,9998
[7 1]	8	2,7E-08	32,7	1
[2 2 1]	5	4,6E-05	32	0,9998
[2 3 1]	6	7,4E-05	32	0,9996
[5 3 1]	9	7,8E-07	33	1
[7 5 1]	13	4,9E-10	33	1
[12 7 1]	20	1,3E-10	32,7	1
[2 2 2 1]	7	5,1E-05	32,7	0,9997
[7 5 3 1]	16	7E-05	33	0,9987

Table 5 shows that the best architectures for each hidden layer were:

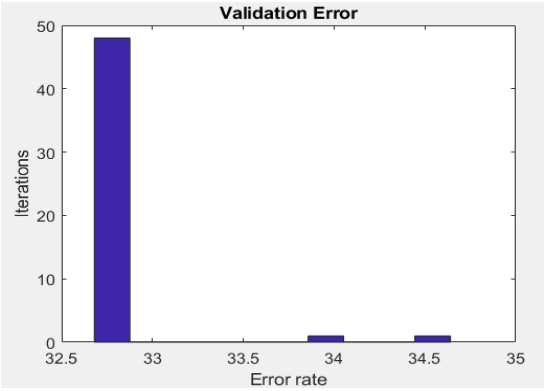

Figure 11. MAE error validation for the best hidden layer architecture of ARC [3 1].

Illustration 11 shows that the architecture of a hidden layer [3 1] has an error rate of 32.7, which means that, out of every 10 people evaluated, approximately three would be wrong in the classification, however, in the case of this architecture because it was trained using the Levenberg-Marquardt algorithm, a decrease in the computational cost was observed, since it took less time to be trained, this is because this optimization algorithm makes higher jumps than the gradient descent algorithm.

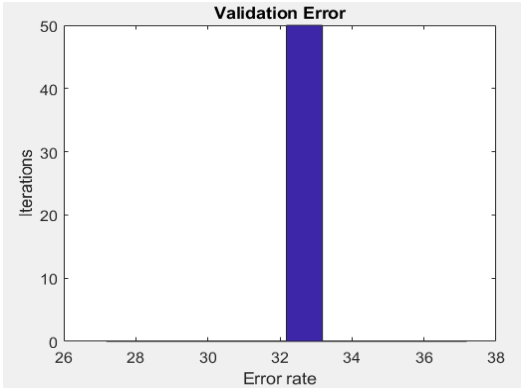

Figure 12. MAE error validation for the best two hidden layer architecture of ARC [2 2 1].

Figure 12 shows that the MAE is 32%, which means that the probability of successful classification is 70%.

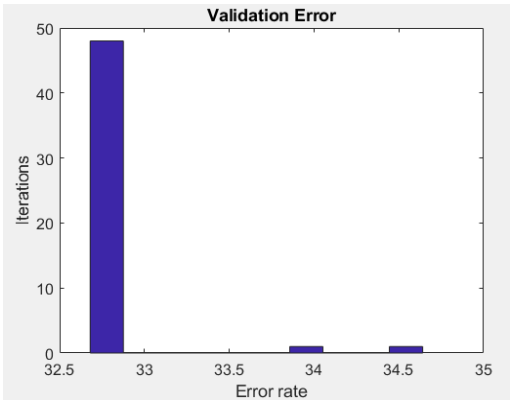

Figure 13. MAE error validation of major two-layer hidden architecture of ARC [2 2 2 1].

Figure 13 shows that the MAE is 32.7%, also that there is a probability of success of 70%, the computational cost was lower in terms of time since it took approximately 30 seconds less to give the result than its counterpart architecture with the gradient descent algorithm.

The best artificial neural architecture tested was [2 2 1], having:

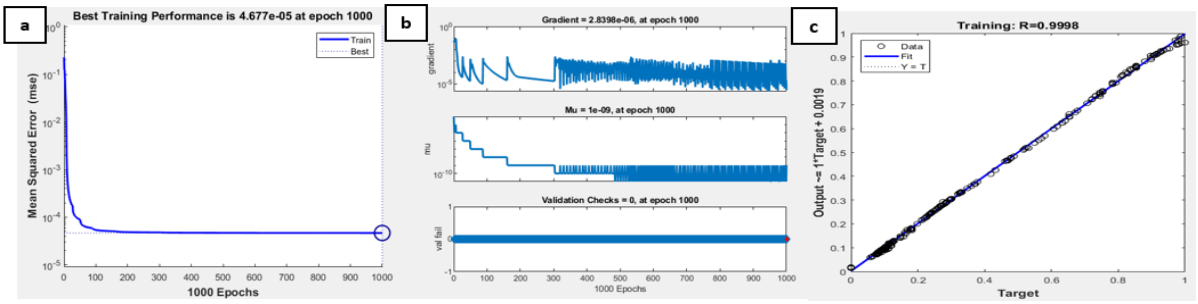

Figure 14. ARC [2 2 1], a) Mean square error MSE=4.67E-15, b) Gradient, validations and learning rate and c) Regression R=0.9998.

5. ANALYSIS AND DISCUSSIONS

The behavior of the training and validation error with respect to the number of neurons of the architectures with only one hidden layer is shown in Table 4, with the following behavior:

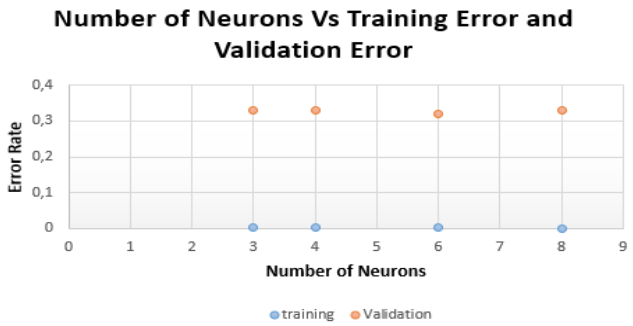

Figure 15. Number of Neurons Vs Training Error and Validation Error

Illustration 15 shows that the validation error remains relatively constant, giving a better response in the use of the architecture [5 1] which had a percentage of 32%, in the other tests the value remained at 33%, in the training error as the number of neurons increased, a slight decrease in the error was observed. Now we proceed to show the behavior of the training and validation error with respect to the number of neurons of the architectures with only one hidden layer, in table 5, having the following behavior:

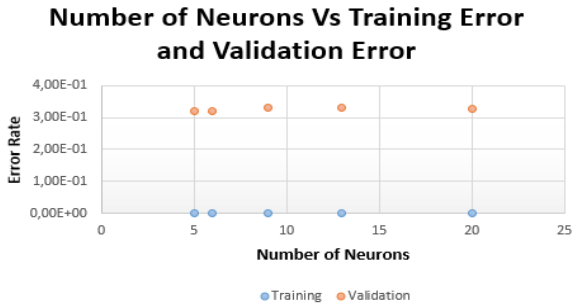

Figure 16. Number of Neurons Vs Training Error and Validation Error

In Figure 16 it was observed that the lowest validation error was generated in the first two architectures, however, the training error was lowest in the [2 2 1] architecture with the MSE being 4.6E-05.

After performing the analysis with different architectures and training algorithms, it was observed that the best architecture is the one given by [2 2 1], since it has a lower number of neurons, which means a lower computational cost, a lower training error (MSE) and a better regression, which allows a better data fit.

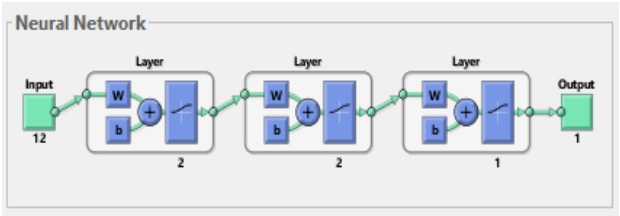

Figure 27. Best Neural architecture found.

The logic followed for the analysis of the neural network generated in the paper is given in the following flowchart:

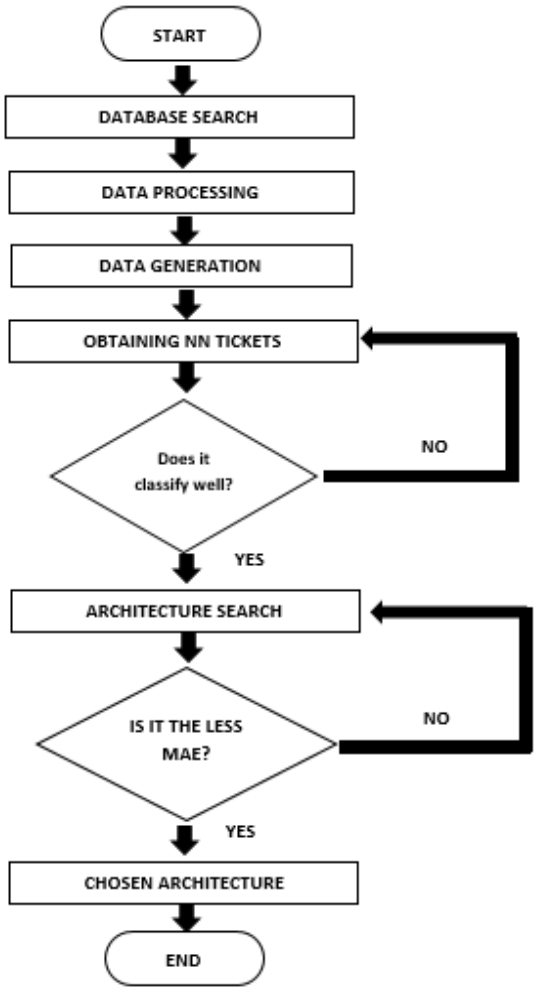

Figure 18. Flowchart

6. CONCLUSIONS

- The best architecture found was [2 2 1] which presented an MSE of 4.6E-05, an MAE of 32% and a regression of 0.999, this was trained with the Levenberg-Marquardt algorithm, which tends a searches for local minima and thereby significantly reduces the computational cost.
- It was observed that the best classification neural network was found with a 32% validation error, which shows that the inputs were not the most appropriate for the generation of the architecture, so in future works an important task is to review in depth the different inputs to use.
- As future work, we will proceed to generate our own database with patient information acquired from the experimental field for the analysis of the median nerve in order to acquire relevant data that will allow us to make a classification network for the prevention of carpal tunnel syndrome.

Author Contributions: The electronic engineer Diego Barragán was in charge of making the neural network, the data treatment and the structure of the article, Dr. Roberto Ferro, was in charge of reviewing the literature and correcting the spelling with Professor Jorge Salamanca, adding some references to strengthen the theoretical framework of the article.

Funding: This research received no external funding.

Institutional Review Board Statement: Not applicable.

Informed Consent Statement: Not applicable.

Data Availability Statement: Data available in a publicly accessible repository. The data presented in this study are openly available in the Machine Learning Repository UCI. Link: http://archive.ics.uci.edu/ml/datasets/sEMG+for+Basic+Hand+movements. Reference: For the database 1),C. Sapsanis, G. Georgoulas, A. Tzes, D. Lymberopoulos, Improving EMG based classification of basic hand movements using EMD • in 35th Annual International Conference of the IEEE Engineering in Medicine and Biology Society 13 (EMBC 13), July 3-7, pp. 5754 - 5757, 2013.For the database 2): C. Sapsanis, Recognition of Basic Hand Movements Using Electromyography, Diploma Thesis, University of Patras, 2013

Conflicts of Interest: The authors declare no conflict of interest.

REFERENCES

1. W. F. U. Rojas, F. M. Santa. “Implementación de un electromiógrafo con interfaz USB”, p. 14, 2012.

2. G. E. Muñoz y G. M. Rebodello. “Electromiografía en las Ciencias de la Rehabilitación”. Revista Salud Uninorte, Vol 34, No. 3, pp. 753-765, 2018.

3. M. E. R. García, G. D. Méndez and M. O. M. Gutierrez. “Development of a Myoelectric-Controlled Prosthesis for Transradial Amputees”. Revista Mexicana de Ingeniería Biomédica. Vol. 38, No. 3, pp. 602-620, doi: dx.doi.org/10.17488/RMIB.38.3.8, 2017.

4. D. Buongiorno, G. D. Cascarano, I. De Freudis, A. Brunetti, L. Carnimeo, G. Dimauro and V. Bevilacqua. “Deep Learning for Processing Electromyographic Signals: a Taxonomy-based Survey”. Journal Pre-proofs. Pages 20, , doi: https://doi.org/10.1016/j.neucom.2020.06.139, 2020.

5. T. Yu *et al*., "Recursive Decomposition of Electromyographic Signals With a Varying Number of Active Sources: Bayesian Modeling and Filtering," in *IEEE Transactions on Biomedical Engineering*, vol. 67, no. 2, pp. 428-440, Feb. 2020, doi: 10.1109/TBME.2019.2914966.

6. J. V. Pinzón, R. P. Mayorga, G. C. Hurtado. “Brazo Robótico controlado por electromiografía”, p. 9,2012.

7. E. Heald, R. Hart, K. Kilgore and P. H. Peckham. “Characterization of Volitional Electromyographic Signals in the Lower Extremity After Motor Complete Spinal Cord Injury”, Vol. 31, No. 6, Pp. 538-591, doi: https://doi.org/10.1177/1545968317704904, 2017.

8. A. V. Moreno, E. G. Gutiérrez, J. C. P. Moreno. “Consideraciones para el análisis de la marcha humana. Técnicas de videogrametría, electromiografía y dinamometría”, vol. 2, p. 11, 2008.

9. Francesco Di Nardo, Alessandro Mengarelli, Annachiara Strazza, Valentina Agostini, Marco Knaflitz, Laura Burattini, Sandro Fioretti, “A new parameter for quantifying the variability of surface electromyographic signals during gait: The occurrence frequency”.Journal of Electromyography and Kinesiology, Vol. 36, pp. 25-33, ISSN 1050-6411, https://doi.org/10.1016/j.jelekin.2017.06.006. 2017.

10. H. Dimitrov, A. M. J. Bull and D. Farina, "Real-Time Interface Algorithm for Ankle Kinematics and Stiffness From Electromyographic Signals," in *IEEE Transactions on Neural Systems and Rehabilitation Engineering*, vol. 28, no. 6, pp. 1416-1427, June 2020, doi: 10.1109/TNSRE.2020.2986787.

11. J. M. Fernández, R. C. Acevedo, C. B. Taberning. “Influencia de la fatiga muscular en la señal electromiográfica de músculos estimulados eléctricamente”, p. 9, 2007.

12. M. Muñoz, M. Gutierrez. “ENTIENDO LA ELECTROMIOGRAFÍA”, POWEREXPLOSIVE, 2016. Enlace: https://powerexplosive.com/entendiendo-la-electromiografia/

13. D. A. B. Vargas, R. F. Escobar. “Estudio de modelos propuestos para el nervio mediano sano y con síndrome del túnel del carpo”. Revista Noria. Vol. 2, p. 15, 2019.

14. D. R. McNeal. “Analysis of a Model for Excitation of Myelinated Nerve”, p. 9, 1976.

15. S. Snarrenberg, B. N. Sevak, J. L. Patton. “Modeling Nerve Compression in Carpal Tunnel Syndrome”, p. 4, 2018.

16. C. T. M. Choi, S. H. Sun. “Simulation of Axon Activation by Electrical Stimulation- Applying Alternating-Direction-Implicit Finite-Difference Time-Domain Method”, vol. 48, p. 4, 2012.

17. R. R. Serrezuela, J. L. A. Trujillo, D. R. Delgado, V. K. O. Benavides, R. S. Zamora, E. M. Reyes. “Diseño e implementación de una prótesis de mano robótica antropomórfica subactuada”, p.8, 2018.

18. B. A. de la C. Sánchez, M. A. Montiel, E. L. González. “Diseño y Construcción de un Prototipo de Exoesqueleto para Rehabilitación de Mano”, p. 4, 2018.

19. H. S. Horace, S. C. S. Chan, M. S. W. Lam. “HACS: Hand Action Coding System for Anatomy-Based Synthesis of Hand Gestures”, p. 6, 1998.

20. H. Hashimoto, A. Sasaki, K. Makino, K. Mitsuhashi. “Reduced DoFs of Digital Hand Based on Anatomy for Real Time Operation”, p.5, 2014.

21. S. O. Villaruel, S. Gutiérrez. “Liberación endoscópica del túnel cubital. Técnica y resultados clínico-funcionales”, p. 5, 2019.

22. F. Martínez, C.Medici, M. Algorta. “SÍNDROME DEL TÚNEL CUBITAL SECUNDARIO A MÚSCULO

ANCONEOEPITROCLEAR: REPORTES DE CASO", p. 4, 2012.

23. S. B. Akben. "Low-cost and easy-to-use grasp classification, using a simple 2-channel surface electromyography (sEMG)", P.6, 2017.

24. Wilmer. "Desafíos de la Inteligencia Artificial Bioinspirada con Algoritmos Genéticos", p. 27, 2017.

25. R. R. Serrezuela, M. A. T. Cardozo, J. J. G. Montiel, R. S. Zamora, E. M. Reyes. "Análisis comparativo entre de MAE y RNA en señales de EMG obtenidas para control de una prótesis de mano robótica", p. 6, 2019.

26. D. H. Susana, F. T. Fraga. "Simulación de una red neuronal con mapas auto-organizados (SOM) de KOHONRN", vol. 3, p. 4, 2017.

27. V. Vázquez, O. Oubram, A. Bassam, V. Aguilar, O. López. "Sistema de reconocimiento inteligente de señales mioeléctricas del movimiento de mano humana", p. 14, 2017.

28. Qingcong Wu, Bai Chen, Hongtao Wu, Neural-network-enhanced torque estimation control of a soft wearable exoskeleton for elbow assistance, Mechatronics, Volume 63, 2019, 102279, ISSN 0957-4158,https://doi.org/10.1016/j.mechatronics.2019.102279.

29. R. A. González, R. E. Ferro, D. Liberona. "Government and governance in intelligent cities, Smart transportation study case in Bogotá Colombia", p. 10, 2019.

30. C. Sapsanis, G. Georgoulas, A. Tzes, D. Lymberopoulos. "Improving EMG classification of basic hand movements using EMD", p. 4, 2013.

31.Y. Yun *et al*., "Maestro: An EMG-driven assistive hand exoskeleton for spinal cord injury patients," *2017 IEEE International Conference on Robotics and Automation (ICRA)*, Singapore, 2017, pp. 2904-2910, doi: 10.1109/ICRA.2017.7989337.

32. M. K. Burns, D. Pei and R. Vinjamuri, "Myoelectric Control of a Soft Hand Exoskeleton Using Kinematic Synergies," in *IEEE Transactions on Biomedical Circuits and Systems*, vol. 13, no. 6, pp. 1351-1361, Dec. 2019, doi: 10.1109/TBCAS.2019.2950145.

33. S. Ghosh and M. F. Orlando, "Continuous Joint Angle Estimation of an Index Finger Exoskeleton using Online EEG Signal," *2019 IEEE/ASME International Conference on Advanced Intelligent Mechatronics (AIM)*, Hong Kong, China, 2019, pp. 808-813, doi: 10.1109/AIM.2019.8868794.

34. J. Kimura. "Electrodiagnosis in diseases of nerve and muscle principles and practice", OXFORD University PRESS, p. 1177, 2013.

35. S. Osuna, J. Gonzalez, A. Ilzarbe. "Procesado de señales EMG en Trastornos Neuromusculares", p. 25, 2013.Enlace:https://www.researchgate.net/publication/271273663 Procesado de senales EMG en Trastornos Neuromusculares